

Frequency-controlled wireless shape memory polymer microactuator for drug delivery application

M. A. Zainal¹ · A. Ahmad¹ · M. S. Mohamed Ali¹

Published online: 26 January 2017
© Springer Science+Business Media New York 2017

Abstract This paper reports the wireless Shape-Memory-Polymer actuator operated by external radio frequency magnetic fields and its application in a drug delivery device. The actuator is driven by a frequency-sensitive wireless resonant heater which is bonded directly to the Shape-Memory-Polymer and is activated only when the field frequency is tuned to the resonant frequency of heater. The heater is fabricated using a double-sided Cu-clad Polyimide with much simpler fabrication steps compared to previously reported methods. The actuation range of 140 μm as the tip opening distance is achieved at device temperature 44 $^{\circ}\text{C}$ in 30 s using 0.05 W RF power. A repeatability test shows that the actuator's average maximum displacement is 110 μm and standard deviation of 12 μm . An experiment is conducted to demonstrate drug release with 5 μL of an acidic solution loaded in the reservoir and the device is immersed in DI water. The actuator is successfully operated in water through wireless activation. The acidic solution is released and diffused in water with an average release rate of 0.172 $\mu\text{L}/\text{min}$.

Keywords MEMS · Microfabrication · Microactuators · Shape memory polymer · LC circuit · Wireless power transfer · Drug delivery device

1 Introduction

Wireless microactuators offer many application opportunities. One of the promising applications is for implantable drug delivery devices, which allow site-specific drug administration. These devices allow drugs to be delivered at a targeted location to increase drug efficiency in order to combat targeted disease such as osteoporosis treatment (Farra et al. 2012), chronic ocular disease (Lo et al. 2009), as well as pain control (Smith et al. 2005). The well-established microfabrication technology has demonstrated outstanding versatility toward building an implantable drug delivery device utilizing microelectromechanical system (MEMS) technology. An MEMS-based implantable drug delivery system can make a significant contribution to a targeted drug delivery mechanism by incorporating features such as control over drug delivery rate, programmable drug schedule, and wireless drug release. Among of the early approaches for wirelessly drug release is to break the sealing membrane of the drug reservoir (Prescott et al. 2006; Smith et al. 2007; Tang et al. 2008). However, this operation is destructive which means there is no way to abort once the release is triggered. Moreover, this device utilizing active circuitry and powered by batteries, making it bulky and more invasive. It is passive operation mechanism that eliminates the need for active circuitry and batteries and is thus advantageous in term of size, cost, longevity, and robustness of the implants. Wireless microactuator using passive actuation have been reported for several mechanisms, including magnetic actuation (Vollmers et al. 2008), an electrostatic force (Basset et al. 2002), bimorph (Han and Chen 2005),

Electronic supplementary material The online version of this article (doi:10.1007/s10544-017-0148-5) contains supplementary material, which is available to authorized users.

✉ M. S. Mohamed Ali
sultan_ali@fke.utm.my

M. A. Zainal
mamri3@live.utm.my

A. Ahmad
anita@fke.utm.my

¹ Faculty of Electrical Engineering, Universiti Teknologi Malaysia, 81310 Skudai, Johor, Malaysia

and shape memory alloy (SMA) (Zaidi et al. 2010). However, they are not compatible for implantable device application and pose various practical issues such as integration with ferromagnetic material, the need for high voltages, small actuation stroke, and complex fabrication/integration processes.

There have been some development efforts using a SMA microactuator in implantable devices (Fong et al. 2015; Mohamed Ali and Takahata 2011). In these reports, bulk-micromachined SMA has been used as actuators which offer desirable features for biomedical application such as high work density, a large force, and biocompatibility. However, they have to go through meticulous fabrication processes such as using electrical discharge machining or etching using hydrofluoric acid to get the desirable shape of SMAs. Furthermore, they also require the high-temperature plasma-enhanced chemical vapor deposition (PECVD) system to deposit stress layer (i.e. SiO_2 , Si_3N_4) on the SMA in order to provide deformation to the actuator. Shape memory polymer (SMP) actuators are promising candidates that eliminate the need for the aforementioned processes. SMP are polymeric materials with shape-memory-effect and they have the ability to change from a temporary shape to a memorized shape due to external stimuli, i.e. heat, light. The temporary shapes are maintained until the appropriate stimulus is applied to the material to induce shape-memory-effect, recovering the memorized shape. In addition, SMPs have unique advantage of being lightweight, inexpensive, low density, good manufacturability, high shape deformability, good biodegradability, and biocompatible. Compare to other shape memory material such as shape memory ceramic and SMA, SMP posses the highest recoverable strain levels. SMPs with one-way shape-memory-effect can only memorize their original shape, and recover from their temporary shape to their original shape once stimulated. An actuator fabricated using SMP will be more useful if it exhibits a two-way shape-memory-effect (TWSME) (H. and G. 2013). However, the fabrication of TWSME SMP such as by using liquid crystalline elastomers or based on the principle of crystallization-induced elongation is complicated approaches (Ahn et al. 2010; Li et al. 2011). An alternative to TWSME to fabricate SMP with two-way actuation capability is by employing SMP-laminate composite. This approach eliminates the need for complicated training processes to make the material memorize TWSME while exhibiting two-way actuation by exploiting bias spring or the coefficient of thermal expansion (CTE) mismatch between SMP and laminated composites (Chen et al. 2008). The driving force behind the two-way actuation here is the release of the elastic strain of the SMP layer upon heating, and the elastic strain recovery induced by the bending force of substrate layer upon cooling (Meng and Li 2013). Later, Tamagawa reported the use of the CTE mismatch between a pure epoxy resin and a fiber-reinforced resin to fabricate another polymeric laminate with two-way actuation behavior (Tamagawa 2010;

Tamagawa et al. 2010). To the best of author's knowledge, only these two works report the behavior and usefulness of the actuator for two-way actuation; there is no experiment to date on the operational of the actuator as a functioning device.

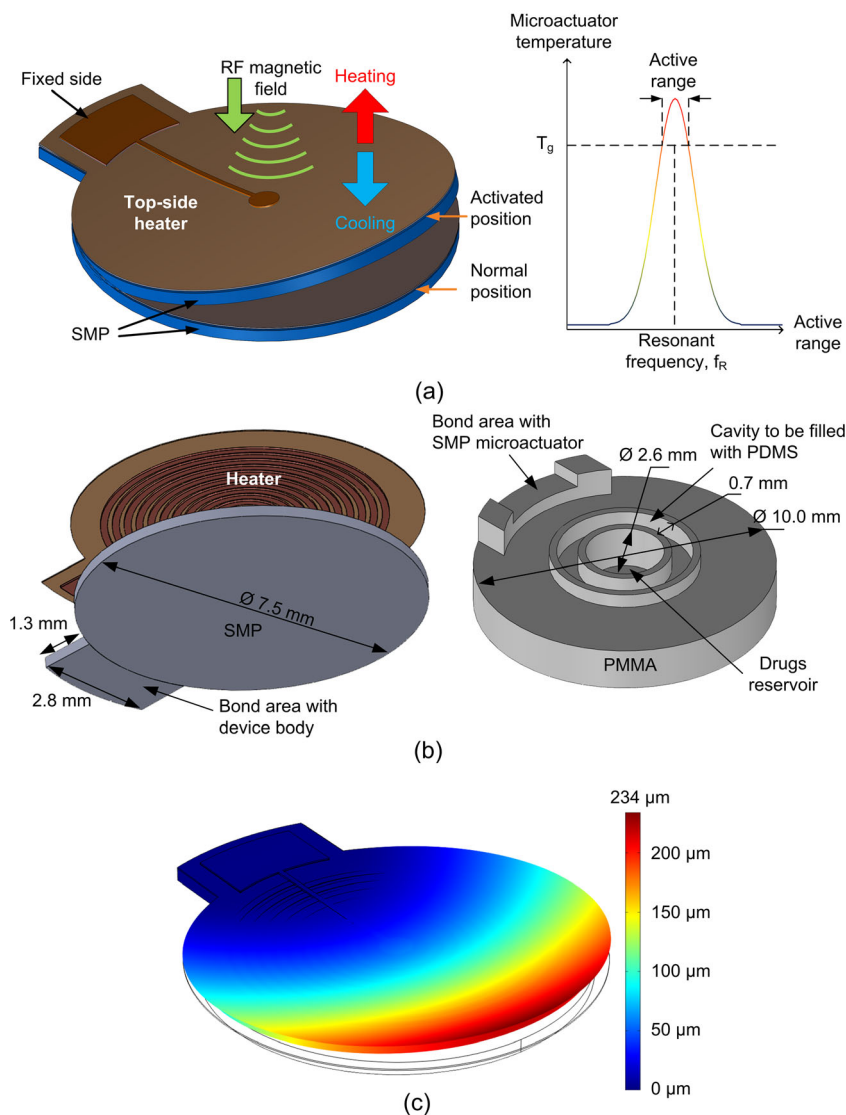
SMPs are usually triggered by thermal stimuli where the actuation is triggered by a magnetic field, laser radiation or by supplying electric current. Recently, there have been reports on using Fe_3O_4 nanoparticles as filler in SMP to activate it magnetically (Feng et al. 2016; Gu et al. 2016). These particles serve as internal mini-antenna to transform the electromagnetic energy to Joule heat through a magnetic field induced heating (Weigel et al. 2009). Although it can be activated wirelessly and Fe_3O_4 has shown a good biocompatibility property (Wang et al. 2016), this kind of SMPs needs to be blended with the filler and is incompatible with bulk-SMP. While the laser activated SMPs require line of sight for their operation (Maitland et al. 2002), using a multiwalled carbon nanotube or carbon black as filler in electrically conducted SMPs composite is impractical in implantable devices (Du et al. 2015; Lu et al. 2014). To this point, a radio frequency (RF) magnetic field to activate thermal actuators (Mohamed Ali and Takahata 2011; Mohamed Ali and Takahata 2010) could be a promising candidate to activate the SMP and at the same time addressing all of the drawbacks mentioned above.

This paper reports an implantable drug-delivery device using an SMP/Polyimide (PI) laminate actuator that exhibits two-way actuation, wirelessly powered and controlled by external RF magnetic fields. The device is designed and fabricated with passive circuitry that is operated without batteries. The thermal responses of the actuators are experimentally characterized. The wireless control of the coloring dye concentration and pH level of the liquid using the fabricated device is performed for demonstration purpose of the developed wireless actuation technique for implantable drug delivery application.

2 Device working principle and design

The device developed in this work utilizes planar inductor-capacitor (LC) resonant circuit as a heater to control the thermoresponsive SMP material as shown in Fig. 1a. The LC circuit is heated when it is exposed to an AC magnetic field with the frequency matching the resonant frequency of the LC circuit caused by the electromotive force induced by the field. The SMP actuator is bonded with the heater fabricated from a Cu-clad PI sheet. This integration forms an SMP/PI structure (Fig. 1b), in which the Cu-clad PI is not only become part of the heat source but also serves as a stress layer that will provide deformation through the bimorph principle. While the SMP is heated above the glass transition temperature, T_g , the material turns into a soft rubbery state due to increased mobility of the molecular chain. This allows easy deformation when an external force is

Fig. 1 **a** Device conceptual diagram, and working principle of frequency sensitive wireless heater, **b** bottom-side isometric view of SMP microactuator with wireless heater, and device body, **c** COMSOL simulation model of the SMP/PI actuator showing approximate displacement of 234 μm when heated to 50 $^{\circ}\text{C}$



applied, and the deformed shape is preserved if the force is maintained while cooling the SMP below T_g . In this work, heating the actuator above T_g allows us to firmly seal the reservoir after the process of bonding the actuator with the device body. The actuator will come into contact with PDMS poured in the cavity (Fig. 1b). The drug is inserted into the reservoir via a small hole drilled on the backside of the device. When the LC circuit is exposed to electromagnetic field frequency, f_m , with the frequency that matches its resonant frequency of the device, f_r , it is heated due to the electromotive force induced by the field (Fig. 1a). This activates the SMP actuator where bends upward due to the mismatch in the CTE between SMP and PI (CTE of SMP is higher than CTE of PI). At this moment, the drug will diffuse out from the reservoir. Upon tuning f_m away from f_r , there is no heat will be generated by the heater and the actuator returns to flat shape and closes the reservoir

preventing further the release. An analysis using a finite element tool (COMSOL Multiphysics™) suggested an acceptable design’s dimension ensure that the actuator provides enough space between actuator and reservoir when actuated (Fig. 1c). The simulation result was obtained by evaluating the thermal expansion undergoes by the actuator when subjected to increasing the temperature. It shows a maximum tip opening of 234 μm using an SMP thickness of 250 μm when the actuator is heated to 50 $^{\circ}\text{C}$.

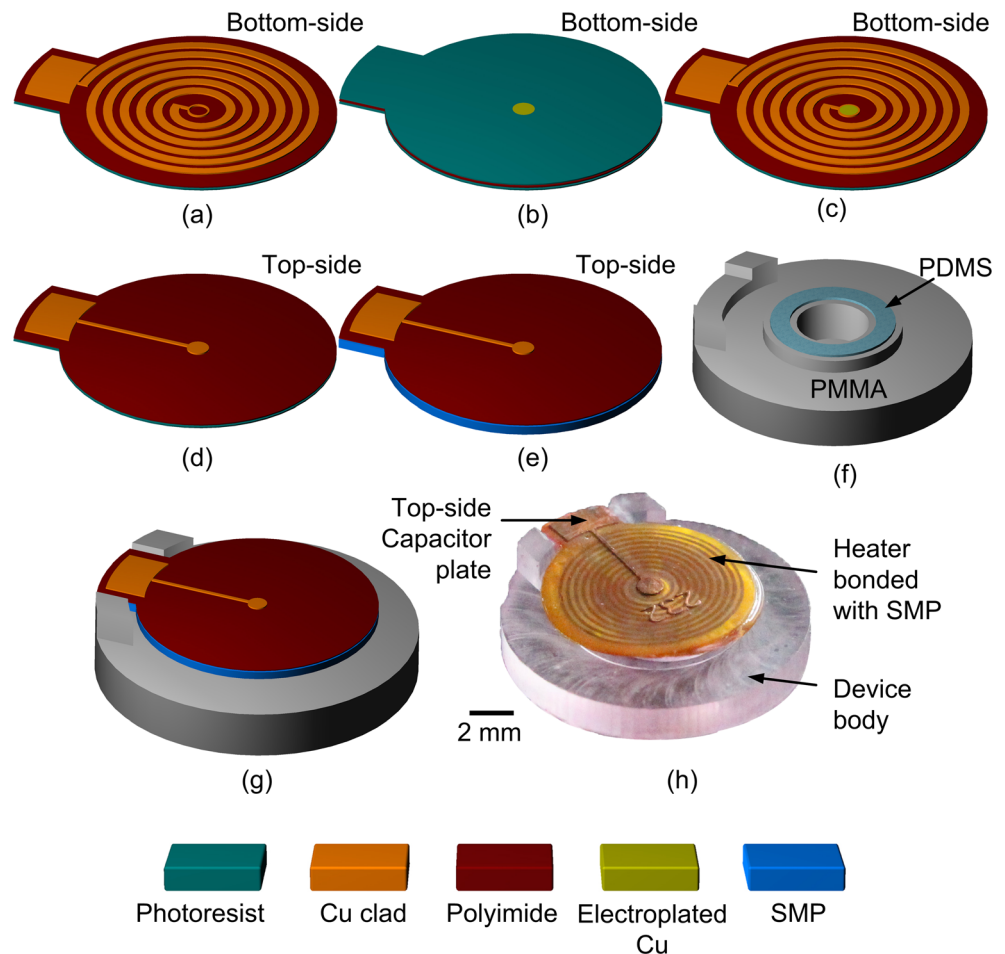
3 Device fabrication

The device body with a diameter of 10 mm is fabricated by micro-machining a 5 mm-thick polymethylmethacrylate (PMMA) extrusion sheet using a micro milling machine (DT110 Mikrotols, Singapore). Then, an amount of

polydimethylsiloxane (PDMS) (Sylgard 184, Dow Corning Corp., Midland, MI, USA) is poured into the PMMA cavity to enhance the reservoir sealing. Fig. 2 (a-g) shows the heater's fabrication process and completed device illustration developed for the device. The planar LC circuit is fabricated using double-sided Cu-clad PI film (Sheldahl G1860) with 35- μm -thick Cu and 25- μm -thick PI. Photolithography for the fabrication is performed with dry-film photoresist (PlateMaster PM240, DuPont, DE, USA). First, the bottom-side of the LC circuit which consist of an inductor (coil) and one capacitor plate is formed by wet etching the of Cu-clad layer (this side will be denoted as 'bottom-side' while the other as 'top-side') using a patterned PM240 photoresist as a mask (Fig. 2a). Next, the via contact is formed by wet etching PI from the bottom-side of the film and Cu electroplating in the patterned photoresist is performed in a Cu_2SO_4 solution at a current density of 29 mA/cm^2 for 20 min (Fig. 2b). The purpose of this step is to make the connection between the top and bottom Cu side of the film. The complete bottom-side of the heater is shown in Fig. 2c after photoresist stripping. Then, the other side of capacitor plate is formed by wet etching of Cu using the patterned photoresist as a mask to

complete the planar LC circuit (Fig. 2d). The SMP actuator is fabricated from a 250- μm -thick SMP sheet with $T_g = 65^\circ\text{C}$ (DiAPLEX MM6520, SMP Technologies Inc., Tokyo, Japan) and is cut using a vinyl cutter (Silhouette CAMEO[®], UT, USA) to get the desired shape. Next, the SMP actuator and the heater are bonded together by gradually heating the SMP on a hot plate gradually with increments of 10 $^\circ\text{C}/\text{min}$ up to 150 $^\circ\text{C}$ for 5 min (Fig. 2e). The bonded SMP and heater are then cooled to room temperature to make the SMP actuator functional. Finally, the SMP actuator is bonded to the drugs reservoir partially utilizing dichloromethane (DCM) as the adhesive. At this point, the SMP actuator functions as an enclosure and seals the drug reservoir. To firmly seal the reservoir, the SMP must be trained by heating the actuator until the temperature reaches slightly above T_g ($\sim 80^\circ\text{C}$). After that, some pressure is applied to the actuator to close the reservoir until the actuator temperature is back to room temperature. During this process, the shape-memory-effect has been utilized to deform the SMP and sealed the reservoir. When it reaches to the room temperature, the drugs reservoir is fully sealed and the device is completed. The device body poured with PDMS in the cavity is illustrated in Fig. 2f while Fig. 2g

Fig. 2 Heater fabrication process (a-e), **a** bottom-side: etch Cu, **b** bottom-side: Cu electroplating, **c** view after completing bottom side, **d** top-side: etch Cu, **e** top-side: bond SMP with bottom-side of completed heaters, **f** device body with PDMS on cavity, **g** illustration of a complete device, **h** fabricated device



illustrated the complete device. The complete fabricated device is as shown in Fig. 2h.

4 Experimental result and discussion

The characterization and experimental results for the fabricated actuators operated by the frequency-modulated RF magnetic field as well as their thermal behavior are discussed in this section. The performance of the drug delivery device is evaluated with a demonstration of the wireless control for a temporal drug release.

4.1 SMP characterization

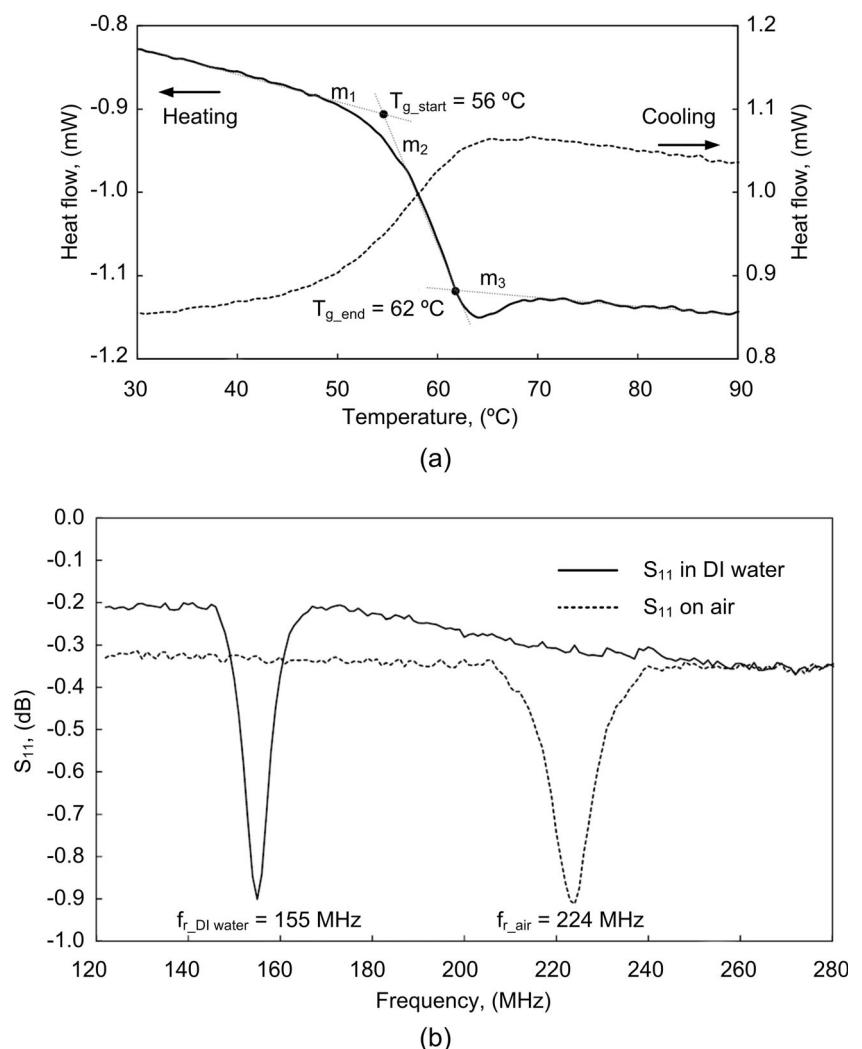
Differential scanning calorimetry (DSC) analysis was used in order to determine the transformation temperature of the SMP. The DSC measures T_g by scanning the amount of heat required to increase the SMP's temperature. The SMP was

scanned at 10 °C/min in both heating and cooling mode. The measurement is presented in Fig. 3a where's the T_g range was determined as the intersection point of tangent line m_1 - m_2 and m_2 - m_3 , starting at $T_{g_start} = 56$ °C and ending at $T_{g_end} = 62$ °C. Within this range, the amount of heat to raise the temperature was dramatically increased. The heat energy boosts the mobility of the polymer chain within the polymer matrix, caused the SMP change from a stiff glassy physical state to a softer rubbery state. The point where this property started was at $T_{g_start} = 56$ °C which is defined as T_g in this paper.

4.2 Thermal response of actuator

The heater will be activated once it is exposed to f_m with a frequency that matches f_r . To determine the f_r of the fabricated device, an S_{11} parameters measurement was performed on air and in DI water using a network analyzer (Hewlett Packard 4396B). The result presented in Fig. 3b shows a dip at

Fig. 3 a DSC curve of SMP, b reflective coefficient, S_{11} measurement of the heater measured on air and in DI water using network analyzer



$f_{r_air} \sim 224$ MHz and $f_{r_DI\ water} \sim 155$ MHz that corresponds to f_r of the heater measured on air and in deionized (DI) water respectively. The discrepancy in the measurement of f_r in a different medium is due to impedance mismatch (different permittivity and permeability) of air and water which affect the LC values and transmitted RF wave.

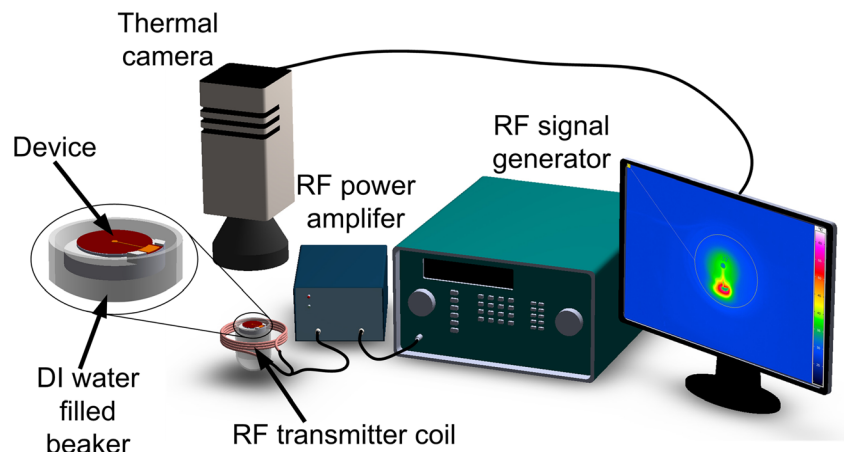
In order to verify the differences in f_r when subjected to water immersion, a wireless heating experiment was conducted using the experimental setup in Fig. 4. The device was immersed in DI water in a beaker. The beaker was placed in the middle of RF transmitter coil. The f_m was tuned starting at 225 MHz down to 100 MHz with a decrement of 1 MHz for every 30 s with RF power of ~ 5 W. The device temperature was recorded using the thermal camera (VarioCAM® HD-07739, SMP, Jenoptic, Jena, Germany). The result presented in Fig. 5a shows that a maximum temperature of 53.5 °C is attained when the f_m is tuned to ~ 153 MHz, which verifies the result presented in Fig. 3b.

The surface area of the SMP is directly bonded to with bottom-side of the heater to provide good heat transfer to the actuator. However, the SMP and PI are known to have low thermal conductivity, which will create a thermal gradient across the actuator due to heat loss and a low heat transfer rate. Hence, it is important to perform spatial and temporal characterization as these are the factors that affect their actuation performance of the heater. To characterize them, the temperature distribution over a period of time was recorded using the thermal camera. The experimental setup used for this experiment is shown in Fig. 4 without the DI water. The actuator was first activated by tuning f_m to 224 MHz. However, by further tuning of the frequency, it was noticed that the maximum heat was generated when f_m was tuned to ~ 218 MHz. The deviation between the measured and actual value was due to the deformation of the actuator that can vary the inductance and capacitance of the wireless heater. The RF power used for this measurement was 0.05 W. Fig. 5b shows a thermal image of the

SMP actuator at 30 s after the activation. Points 1, 2 and 3 in Fig. 5b were measured to be 55.3 °C, 45.0 °C, and 37.1 °C respectively. Points 1 and 2 were inside an area covered by the heater's coil which was the reason that their temperature was higher than point 3. Thus, designing a heater's coil to cover as much area as possible is important to achieve better thermal distribution on the SMP actuator. The characterization of thermal the response for the actuator was further conducted, this time when it was subjected to different RF power. An RF power of 0.05 W, 0.10 W, and 0.15 W were used to activate the heater, and their temperature was recorded. Fig. 5c shows the response of the actuator activated for 30 s measured on point 1 (Fig. 5b). The temperature increases linearly when the RF power was increased. Slopes 2 and 3 (~ 14 °C/s) which are steeper than slope 1 (~ 3 °C/s) suggested that the heating rate with RF power of 0.10 W and 0.15 W was higher than 0.05 W. The increment from 0.05 W to 0.10 W affected the heating rate exponentially. Further increment beyond 0.10 W, show the less significant effect on the heating rate. However, the 0.05 W of an RF power was insufficient to raise the heater's temperature to T_g . Thus, selecting the appropriate RF power is necessary to optimize power efficiency and at the same time good enough to move up the temperature up slightly above T_g . In the case of a medical implant, the optimum RF power is essential so it does not exceed the specific absorption rate of the human body and to prevent thermal damage to living tissue.

An experiment was also conducted to characterize the displacement of the actuator. The actuator was activated in two sets of on/off cycles: 30 s on, 1 min off (set 1), and 10 s on, 1 min off (set 2) with an RF power of 0.05 W. The displacement at point 3 (Fig. 5b) of the actuator was recorded using laser displacement sensor (LK-GD500, Keyence, IL, USA) is shown in Fig. 6. As can be seen in Fig. 6a, the first cycle recorded 326 μ m of displacement on the 30th second of activation. However, the actuator did not recover to the initial

Fig. 4 Experimental setup for wireless test



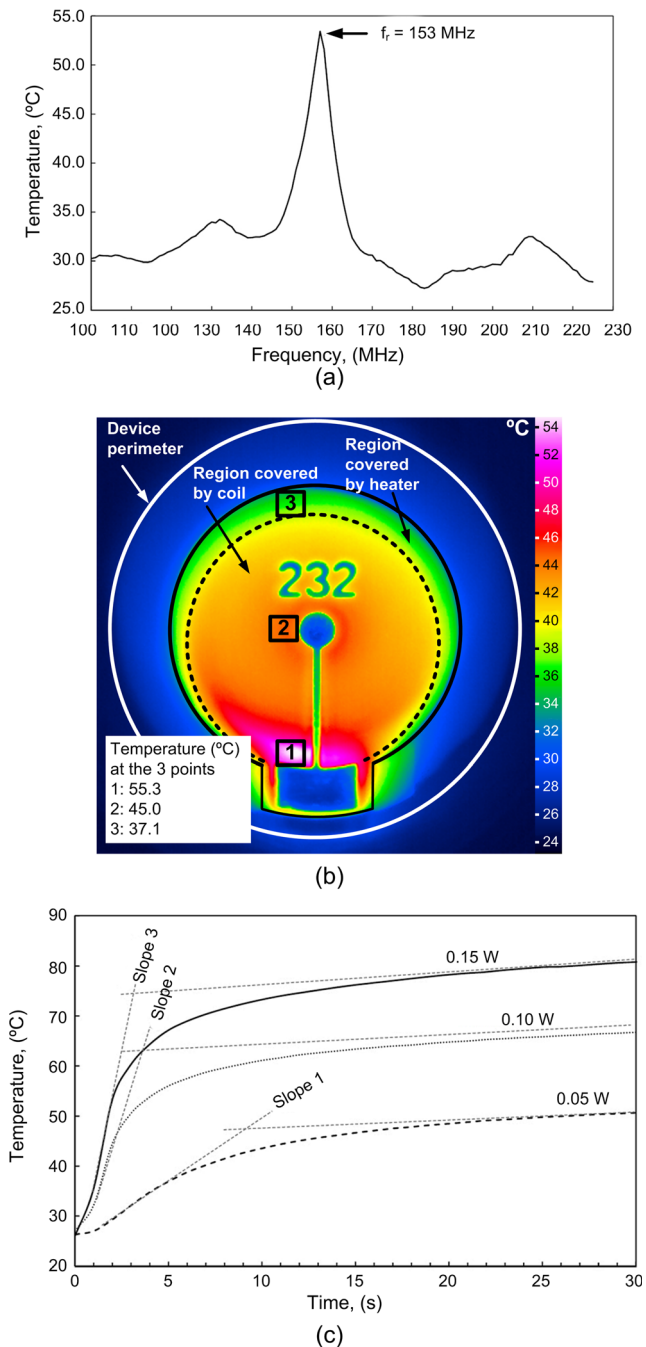


Fig. 5 **a** Thermal response of the heater when subjected RF power of 0.05 W in DI water, **b** thermal image showing the heat distribution of the actuator after 30 s activation with 0.05 W of RF power on air, **c** temporal changes in the temperature when the heater is wirelessly resonated with different RF output power of 0.05 W, 0.10 W, and 0.15 W respectively on air

position, and instead it stayed at 142 μm at the end of off-cycle. This behavior continues until the end of the experiment with recorded values of 180 μm and 192 μm for the second and third cycle respectively. Apart from this, the set 2 on/off cycles shows more favorable results (Fig. 6b). The actuator recovered to ~ 0 μm from cycle 1 to cycle 3. The displacements measured at every end of the on-cycles were 107 μm ,

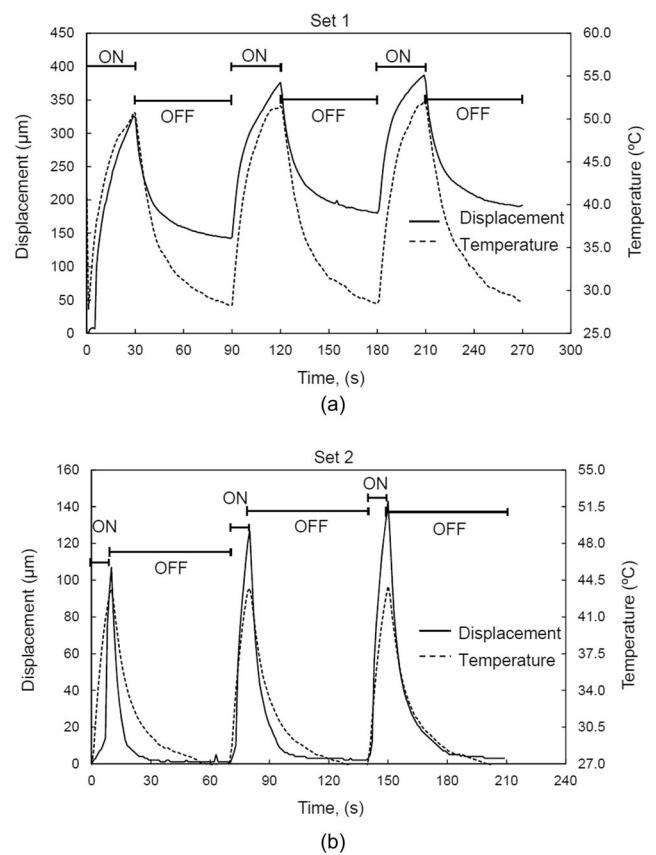
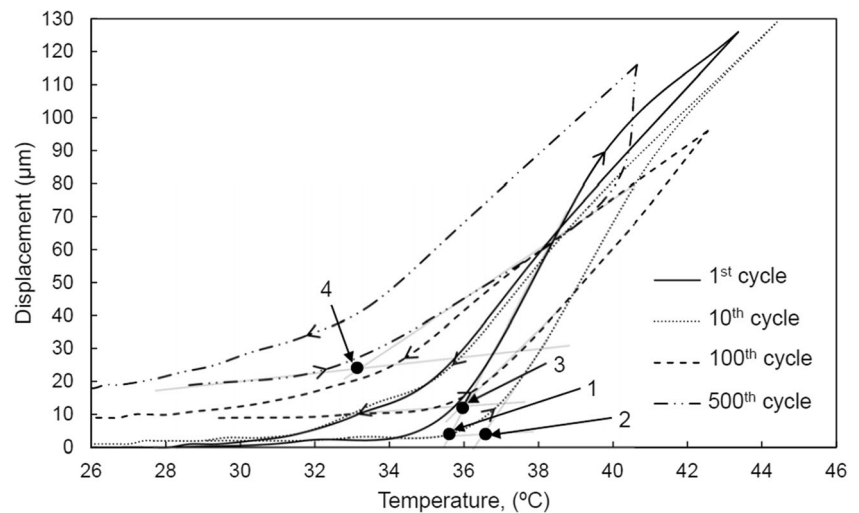


Fig. 6 **a** Actuator displacement and temperature vs. time with response to 30 s on / 1 min off activation, **b** actuator displacement and temperature vs. time with response to 10 s on / 1 min off activation

127 μm , and 143 μm respectively. These experiments suggest that it is necessary to optimize the temperature of the actuator in order to maintain the actuator's integrity. It can be attained by selecting the right value for the RF power level and activation time. Nevertheless, it was also obvious that in set 1 (Fig. 6a) the actuator failed to regain its shape at 0 μm point upon cooling contrary with set 2 (Fig. 6b). One of the reasons could be that in some part of the SMPs, their actual temperature had exceeded T_g . The thermal camera only captured an infrared wave from the PI surface, and it is known that the heat was generated at the heater's coil that is in contact with SMP. Most of the polymeric material will undergo changes in properties above T_g including storage modulus. This is not an exception for SMP, which has lower modulus above T_g . At this point, the stress provided by the PI (including the Cu coil and capacitor plate) was enough to force the SMP to reshape into their new shape.

An endurance test for the developed device was conducted and is presented in Fig. 7. It shows the actuation temperature deviation subjected to 500 cycles of 10 s on / 30 s off period. The figure was plotted at 1st, 10th, 100th, and 500th cycles. From the graph, the displacement of the actuator was increased linearly starting at 33 $^{\circ}\text{C}$ –36 $^{\circ}\text{C}$. Then as the

Fig. 7 Repeatability test subjected to 500 times actuation cycle. The RF power output is 0.05 W with 10 s / 30 s on / off period



temperature further increased, maximum displacement was achieved at a temperature of 40 °C to 45 °C in 10 s activation before cooling during the off period close to room temperature. There is slight variation in the actuation start temperature observed due to the fluctuation of the room the temperature (22 °C – 25 °C), in which affects the actuator displacement as well. The points 1, 2, 3, and 4 in the graph represent the actuator's temperature deviation during on period of 1s, 10th, 100th, and 500th cycles respectively which is measured at the intersection between 2 tangential line. At this point, the actuator started to displace significantly. It shows that as the cycles increases, the temperature needed to initiate the actuator is decreasing. Despite this, the actuator shows a good repeatability having an average maximum displacement of 110 µm with a standard deviation of 12 µm.

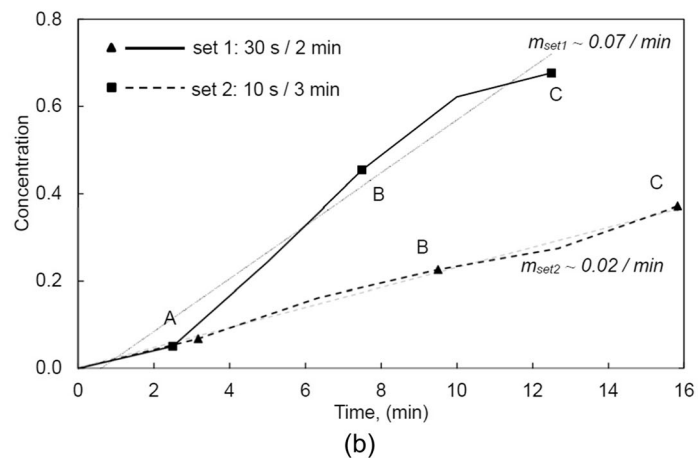
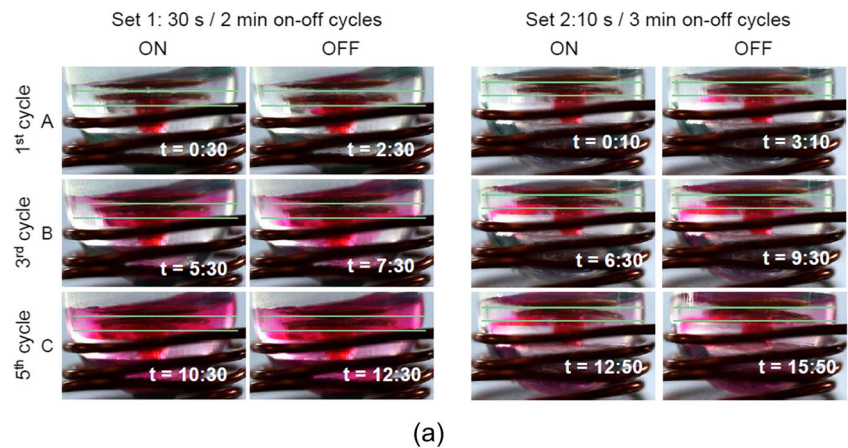
4.3 Wireless release demonstration

Preliminary wireless tests for the fabricated devices were performed by filling the drug reservoir with 5 µL of food-coloring dye. The experimental setup used is shown in Fig. 4. The f_m was tuned to ~153 MHz with an output power of ~5 W. The device was subjected to two sets of on/off cycles: (1) 30 s on, 2 min off; (2) 10 s on, 3 min off and the results are shown in Fig. 8. In set 1, visible dye release was noticed at the end of the first off cycle (Fig. 8a). These activation cycles were continued (Fig. 8a, b), and it can be visually observed a significant amount of dye released at the end of the fifth cycle (Fig. 8a, C). The dye was diffused in DI water in every off-cycle. In set 2 (Fig. 8a, b), less dye release was observed compared to the result in the set 1. This is likely because of DI water temperature is different between set 1 and 2. The device in set 1 was activated 20 s longer than the device in set 2, which indirectly increased the water temperature. The higher water temperature will

require a longer time for the actuator to close the drug reservoir during the off-cycle compared with the lower water temperature. Faster operation while deactivating the actuator will create some pressure on the upper surface of the reservoir, which in turn will squeeze out some of the dye. This behavior was clearly observed during the experiment. Fig. 8b shows a quantitative analysis of the dye concentration versus time for both experiments for sets 1 and 2. The concentration was analyzed using a MATLAB® image processing toolbox in which the pure dye color concentration and DI water were defined as 1 and 0 respectively. In the graph, the grayed color on each line represents linear interpolation for both results. The average increment rate of concentration is calculated as $m_{set1} \sim 0.07$ /min and $m_{set2} \sim 0.02$ /min for set 1 and set 2 respectively. The dye concentration for set 1 (0.68) is higher than set 2 (0.37), even with a shorter total experiment time (set 1: 12.5 min, set 2: 15.83 min). This higher concentration is caused by a longer activation time compared with set 2. These experiments indicate that the actuator properly responded properly to RF magnetic frequency for the controlled release.

The device was further tested to measure the amount of drug released once the device was activated by using a pH buffer. This was carried out by allowing the diffusion of pH buffer from the device reservoir into DI water. The reservoir was filled with 5 µL of the pH 2 buffer solution through the inlet on the back side of the device and sealed using silicone. Then the device was immersed in 10 mL of DI water, and its pH value during the test was measured every 2 min when the RF power of 5 W was turned on continuously for 10 min. The measured pH value and amount of buffer solution released calculated from the pH reading are shown in Fig. 9. The pH measurement indicates a stable reduction from the pH value of 7.0 to the final value of 5.45 due to the release of the pH buffer solution.

Fig. 8 Captured images for ending interval of on-off cycles, **a** set 1: 30 s / 3 min on-off cycles, **b** set 2: 10 s / 2 min on-off cycles, **c** color concentration vs. time (min)



There was an amount of 3.28 μL buffer solution remaining in the reservoir at the end of the experiment with an average release rate of 0.172 $\mu\text{L}/\text{min}$. This value shows that more than half of the liquid remained in the reservoir after 10 min, which is in good agreement with on-off cycle test; from visual observation, there was still some dye remaining at the end of experiments (Fig. 8a, c). Further activation of the device will make the liquid in the reservoir diffuse to DI water over the time in accordance with Fick's law (Fick 1855).

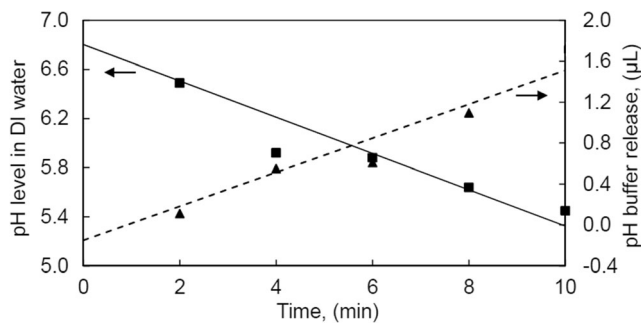


Fig. 9 pH changes (measured) and released amounts of pH buffer (calculated) vs. actuator activated time

5 Conclusion

The first prototype for the proof-of-concept study of a wireless implantable drug delivery device operated by SMP/PI laminate bimorph actuator has been demonstrated. An SMP-integrated with a wireless resonant heater has been realized, in which it is activated selectively using an external magnetic field modulated to the heater's resonant frequency. The T_g of SMP has been measured and was analyzed using DSC. The temporal response and thermal behavior of the actuator were experimentally characterized at different frequencies and RF-power levels. The device successfully showed their operation wirelessly, demonstrated in the water with RF power of 5 W. The release test using a pH buffer and coloring dye has been quantified and reported with an average release rate of 0.172 $\mu\text{L}/\text{min}$. The wireless operation of the device was also implemented to show its ability of controlled released by varying the on-off cycle of the device. The heater which was fabricated using Cu-clad PI was proven to require only a few steps, thus reducing the extra steps required as reported in previous work (Mohamed Ali and Takahata 2011; Mohamed Ali and Takahata 2010). A simple integration of SMP/PI laminate by bonding both materials at temperatures up to 150 $^{\circ}\text{C}$,

shows no sign of mechanical damage, hence eliminating the use of a special chemical as an adhesive. Further work will involve the design and fabrication optimization to miniaturize the device, and to use SMPs with lower T_g and a low-loss transmitter with a lower voltage standing wave ratio to increase the power transfer efficiency. In addition, we look forward to make the heater fully biocompatible by replacing Cu and DCM with biocompatible materials. A forced drug release may be accomplished using micropumps realized by the SMP/PI laminate actuator approach.

Acknowledgements The authors acknowledge the financial support from Ministry of Science, Technology and Innovation Malaysia under E-science Fund (03-01-06-SF1211) and Ministry of Higher Education Malaysia (MOHE) under PRGS (1/13/TK04/UTM/02/01) and FRGS (2/2014/TK01/UTM/02/3) schemes. M. A. Zainal acknowledges the financial support from Universiti Teknologi Malaysia (UTM) under Zamalah scheme.

References

- S.K. Ahn, P. Deshmukh, R.M. Kasi, *Macromolecules* **43**, 7330 (2010)
- P. Basset, A. Kaiser, P. Bigotte, D. Collard, and L. Buchailot, in *Micro Electro Mechanical Systems*, 2002. The Fifteenth IEEE International Conference (2002), pp. 606–609
- S. Chen, J. Hu, H. Zhuo, Y. Zhu, *Mater. Lett.* **62**, 4088 (2008)
- F.P. Du, E.Z. Ye, W. Yang, T.H. Shen, C.Y. Tang, X.L. Xie, X.P. Zhou, W.C. Law, *Composites Part B Engineering* **68**, 170 (2015)
- R. Farra, N.F. Sheppard Jr., L. McCabe, R.M. Neer, J.M. Anderson, J.T. Santini Jr., M.J. Cima, R. Langer, *Sc. Transl. Med.* **4** (2012)
- X.Q. Feng, G.Z. Zhang, Q.M. Bai, H.Y. Jiang, B. Xu, H.J. Li, *Macromolecular Materials Engineering* **301**, 125 (2016)
- A. Fick, *Annalender Physik* **170**, 59 (1855)
- J. Fong, Z. Xiao, K. Takahata, *Lab Chip – Miniaturisation Chemistry Biology* **15**, 1050 (2015)
- S.Y. Gu, S.P. Jin, X.F. Gao, J. Mu, *Smart Mater. Struct.* **25** (2016)
- L.H. Han, S. Chen, *Sensors Actuators, A: Physical* **121**, 35 (2005)
- J. Li, W.R. Rodgers, T. Xie, *Polymer* **52**, 5320 (2011)
- R. Lo, P.Y. Li, S. Saati, R.N. Agrawal, M.S. Humayun, E. Meng, *Biomed. Microdevices* **11**, 959 (2009)
- H. Lu, Y. Yao, L. Lin, *Pigment Resin Technology* **43**, 26 (2014)
- D.J. Maitland, M.F. Metzger, D. Schumann, A. Lee, T.S. Wilson, *Lasers Surgery Medicine* **30**, 1 (2002)
- H. Meng and G. Li, *Polymer(United Kingdom)* **54**, 2199 (2013).
- M.S. Mohamed Ali, K. Takahata, *Sensors Actuators A: Physical* **163**, 363 (2010)
- M.S. Mohamed Ali, K. Takahata, *J. Micromech. Microeng.* **21** (2011)
- J.H. Prescott, S. Lipka, S. Baldwin, N.F. Sheppard Jr., J.M. Maloney, J. Coppeta, B. Yomtov, M.A. Staples, J.T. Santini Jr., *Nat. Biotechnol.* **24**, 437 (2006)
- T.J. Smith, P.J. Coyne, W.R. Smith, J.D. Roberts, V. Smith, *American Journal Hematology* **78**, 153 (2005)
- S. Smith, T.B. Tang, J.G. Terry, J.T.M. Stevenson, B.W. Flynn, H.M. Reekie, A.F. Murray, A.M. Gundlach, D. Renshaw, B. Dhillon, A. Ohtori, Y. Inoue, A.J. Walton, *IET Nanobiotechnology* **1**, 80 (2007)
- H. Tamagawa, *Mater. Lett.* **64**, 749 (2010)
- H. Tamagawa, K. Kikuchi, G. Nagai, *Sensors Actuators, A: Physical* **163**, 356 (2010)
- T.B. Tang, S. Smith, B.W. Flynn, J.T.M. Stevenson, A.M. Gundlach, H.M. Reekie, A.F. Murray, D. Renshaw, B. Dhillon, A. Ohtori, Y. Inoue, J.G. Terry, A.J. Walton, *IET Nanobiotechnology* **2**, 72 (2008)
- K. Vollmers, D.R. Frutiger, B.E. Kratochvil, B.J. Nelson, *Appl. Phys. Lett.* **92** (2008)
- Y. Wang, R. Zhao, S. Wang, Z. Liu, R. Tang, *Biomaterials* **75**, 71 (2016)
- T. Weigel, R. Mohr, A. Lendlein, *Smart Materials Structures* **18**, 025011 (2009)
- S.S. Zaidi, F. Lamarque, J. Favergeon, O. Carton, C. Prella, M. Lejeune, A. Zeinert, *Journal Intelligent Material Systems Structures* **21**, 175 (2010)